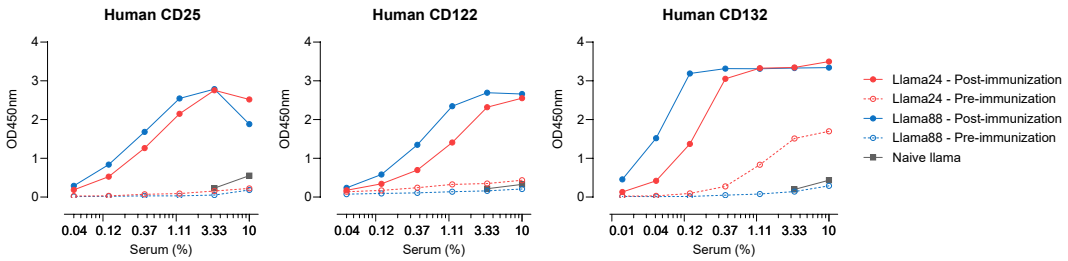

Extended Data Fig. 1 | **Llama immune response.** Specific immune responses to human IL-2Rα/CD25, IL-2Rβ/CD122 and IL-2Rγ/CD132 were measured by ELISA using pre- and post-immune sera on coated recombinant proteins.

a

First injected αVHH

Second injected αVHH	no VHH	αVHH-1	αVHH-4	αVHH-6	αVHH-9	αVHH-3	αVHH-11	αVHH-12	αVHH-2	αVHH-8	αVHH-5	αVHH-10
αVHH-1	72.7	-0.6	0.2	0.3	4.5	26.5	24.3	27.2	52.8	47.6	46.3	32.8
αVHH-4	59.4	8.1	3.1	9.7	6.7	31.4	32.2	31.2	51.0	47.7	53.1	42.8
αVHH-6	53.8	-0.3	0.6	0.3	2.5	19.7	23.5	22.7	43.2	40.6	43.7	36.7
αVHH-9	42.6	3.1	3.2	3.6	5.0	24.4	28.2	27.6	49.6	47.6	54.4	43.4
αVHH-3	29.6	-10.0	-0.8	-7.6	1.7	8.9	13.2	13.7	22.7	27.8	29.0	17.6
αVHH-11	33.3	-6.9	3.4	-4.7	4.1	13.2	11.7	11.5	14.1	18.3	22.8	14.8
αVHH-12	28.8	-7.3	4.6	-4.4	5.4	13.7	11.6	11.4	15.0	18.8	23.3	16.1
αVHH-2	89.9	68.4	80.3	48.1	79.1	86.1	74.5	74.7	-0.2	-4.1	32.4	53.4
αVHH-8	85.1	65.0	77.0	57.6	71.3	74.7	71.6	72.8	10.4	-0.5	32.6	61.4
αVHH-5	36.7	36.6	45.9	27.0	45.6	45.9	45.0	43.4	-4.5	-4.0	11.8	9.4
αVHH-10	101.6	81.4	97.8	85.0	97.7	101.1	95.6	97.7	82.5	91.1	97.3	1.3

Bin	CDR1	CDR2	CDR3
Ia	THNMG	AISWNVDNTLYADSVKG	DNIPLSSDVAATATEYDY
	TRNMG	AVSWNVDNKLYADSVKG	DNIPLSSDMRPTATEYDY
	SYAMG	VISWNVDNTEYTDSVKG	DSIPLSSDMSPTATEYGY
	TYNMG	GTLWSGGDSVYADFAKG	DPLSLTSDWRVDELSS
Ib	SYSMA	AISSSGVVTHVLDSVKG	TASSYSTYEANYNY
	GYAIG	YITGSDGTTYYINSVKG	DRLGSQGRYASAWWRSGDMDL
	GYAIG	YITGSDGSTYYADSVKG	DRLGSRGAYVPIWWRSSDMDL
II	NNFMS	TISYGGESTTYAESVKG	ATSYDSIRSGS
	NNFMS	TISYGGESTTYAEAVKG	ATSYTSIRGAP
III	TWSMA	TISYGGESTTYAESVKG	DRTGVGTNDYNY
	NYAMG	ARDLEGIITRYGDSVKG	RDGGVVAGSRSSAQYNY

No mutual binding — Partial binding — Strong mutual binding

b

First injected βVHH

Second injected βVHH	no VHH	βVHH-15	βVHH-22	βVHH-20	βVHH-16	βVHH-24	βVHH-18	βVHH-17	βVHH-19	βVHH-23	βVHH-26
βVHH-15	37.7	2.1	6.7	12.3	20.4	17.6	24.2	29.8	36.4	31.8	34.9
βVHH-22	33.4	2.6	5.2	10.9	12.8	15.9	21.2	29.9	30.1	22.4	29.8
βVHH-20	24.8	-1.1	1.4	4.8	2.9	9.2	12.8	22.1	19.9	18.5	22.3
βVHH-16	13.7	-2.0	1.7	3.3	5.7	6.8	9.8	15.6	15.7	12.7	17.1
βVHH-24	22.7	-0.9	1.5	5.2	6.2	7.3	8.7	18.5	17.6	14.2	17.9
βVHH-18	13.2	-3.3	-0.4	1.4	2.4	4.3	4.8	8.8	9.3	5.2	9.7
βVHH-17	6.8	1.3	3.9	4.8	5.5	5.0	4.5	-1.1	3.4	-3.8	-0.3
βVHH-19	32.5	30.8	31.5	31.0	34.1	31.1	33.7	34.2	7.7	28.7	32.1
βVHH-23	37.8	33.0	31.3	37.3	35.7	35.2	36.2	32.3	33.7	3.1	3.8
βVHH-26	39.2	33.7	34.6	37.7	36.1	36.6	37.3	33.5	35.7	3.7	4.3

Bin	CDR1	CDR2	CDR3
I	NYAMS	SITGFGRGTDYADSVKG	YSSSTYYPPTPARGRDY
	INAMA	AISRDGGASVYRDSVKG	TRAIGWTARWITTDFDF
	SYAMG	AITWTKRSTDFPDSVKG	ARGLPVTPLGDIIY
	NYPVG	AITWISGSTLYADSVKG	ALKTITRGQNDYSY
	NANMA	LITWSSGSTLYADSVKG	DGPPYSGTYYRYDTYDY
II	SYGIG	CMSRSDDRTYYADSVKG	VDAYGCSLVQPTTYDF
	INGMA	AISRVGNTAYGDSVKG	DSWGGDDY
III	RDAMA	LISWSGATTNYADSVKG	DRRPMGSRSYFEPTEYDD
IV	RYTMA	SVTDSGRTTDYVHSVKG	NTDYFQIKSLDANT
	RYTMA	SVTDSGRTTEYVDSVKG	NTDYFQIRSLDLNT

No mutual binding — Partial binding — Strong mutual binding

c

First injected γVHH

Second injected γVHH	no VHH	γVHH-35	γVHH-28	γVHH-34	γVHH-36	γVHH-37	γVHH-38	γVHH-27	γVHH-29	γVHH-31	γVHH-32
γVHH-35	2.1	-0.9	-7.7	-2.7	-2.9	-1.6	-1.1	-0.1	-2.2	-16.5	-24.0
γVHH-28	29.7	7.9	1.7	1.3	7.9	4.7	8.9	20.6	25.6	6.2	-8.1
γVHH-34	11.7	20.2	6.6	2.8	9.7	6.0	11.3	30.9	32.6	13.2	-0.4
γVHH-36	24.4	15.9	0.9	0.5	4.6	3.1	7.4	15.1	12.9	-4.7	-13.2
γVHH-37	25.4	21.6	7.6	2.6	9.3	6.5	11.4	23.3	21.4	0.1	-8.0
γVHH-38	21.5	21.1	-0.9	0.2	5.0	2.8	11.1	10.9	9.6	-7.9	-15.8
γVHH-27	8.6	3.0	-5.1	3.4	5.5	6.3	6.2	0.6	-0.6	-10.6	-18.4
γVHH-29	12.8	6.4	-2.5	4.7	6.0	4.7	6.8	2.0	1.0	-8.3	-16.0
γVHH-31	33.0	28.1	19.8	25.5	26.7	27.1	27.9	29.1	27.9	2.4	9.5
γVHH-32	64.6	61.1	59.2	60.3	59.5	59.8	59.9	67.6	64.4	49.0	0.9

Bin	CDR1	CDR2	CDR3
I	SYAMG	AISRSGRSTNYADSVKG	GRYYNSAYDPSPGDFGS
II	RYAMG	ANSWGGDTYYADSVQG	APTSFATTAYSGSNSYAY
	RLAMG	VNSWGGDTFYADSVEG	APTSFATTAYSSSNSYAY
	RYAMG	ASSWGGDTFYADSVEG	APTSFPTTAYSSSNSYAY
	RYAMG	IDSWGGDTFYADSVEG	APTSFATTAYSSSNSYRY
	RDAMG	VMSWGGDTFYTDSVEG	APTSFATTAYSSSNSYSY
III	TDVVG	SISRSGDGIYYDDSVKG	GDGWSTYDY
	NYYMG	GIIWNGDHTAYADSIKG	TFWIERATTPDIGQYAY
IV	GYALG	RINWSGSFTYYASSVKG	DNPSTLATDYDN
V	STAVG	AINRSGSATTYADSVKG	DSLPYGRPYYFQRSAGEYDY

No mutual binding — Partial binding — Strong mutual binding

Extended Data Fig. 2a-c | Epitope binning of anti-IL-2R VHH antibodies.
a-c, Epitope binning was performed by surface plasmon resonance (SPR) to assess whether individual VHHs targeting CD25 (**a**), CD122 (**b**), or CD132 (**c**) recognize overlapping or distinct epitopes. Human IL-2R subunits were immobilized on a Biacore CM5 sensor chip, and antibodies were injected sequentially: the first VHH for 2 minutes, followed by a second VHH. An increase in response units (RU) upon the second injection indicates recognition of a non-overlapping epitope. Heatmaps display RU increases at the time of the second injection, enabling identification of four, four, and five discrete epitope bins for CD25, CD122, and CD132, respectively. The CD25 bins matched those obtained via flow cytometry-based binning (panel **d**).

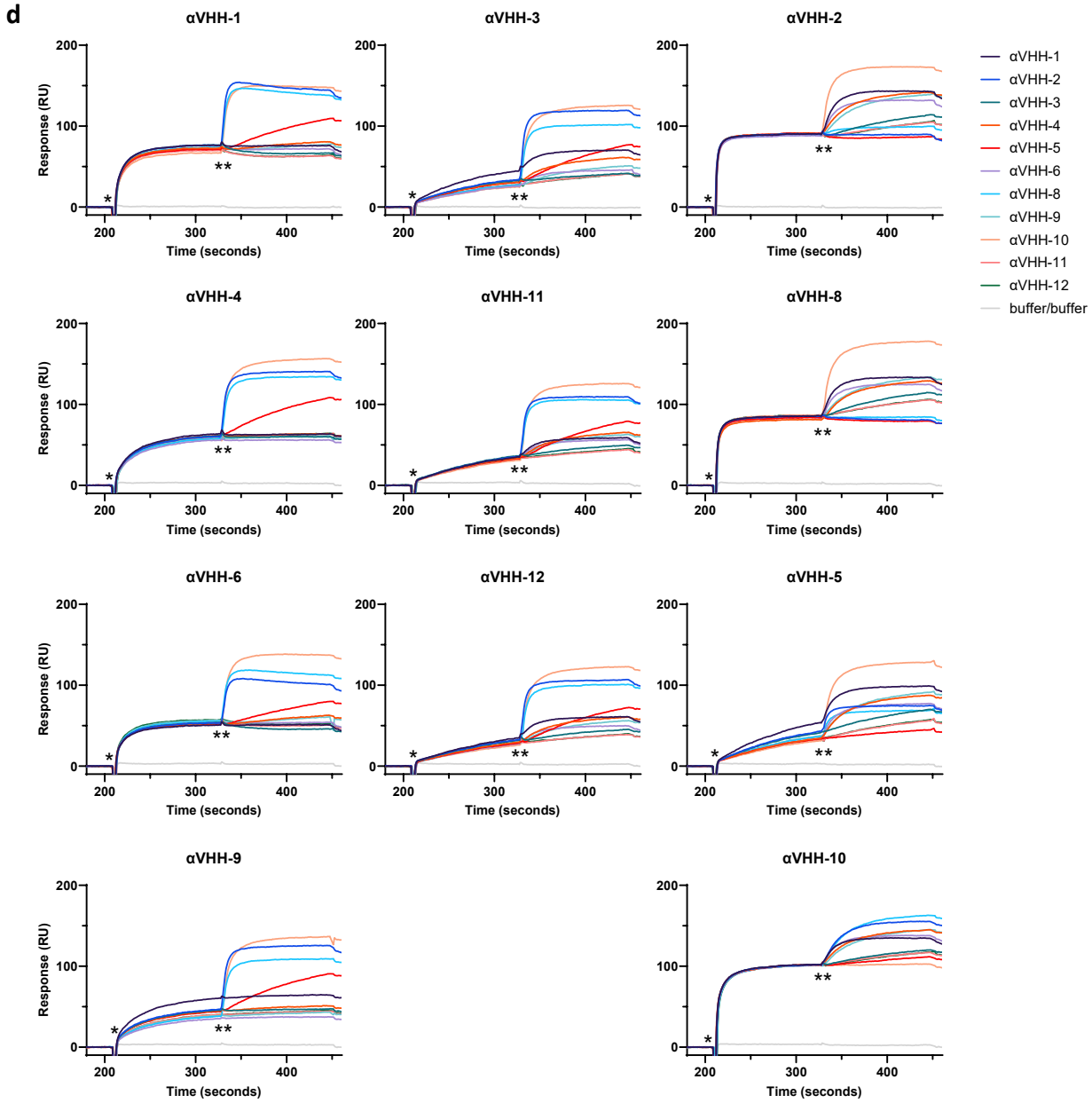

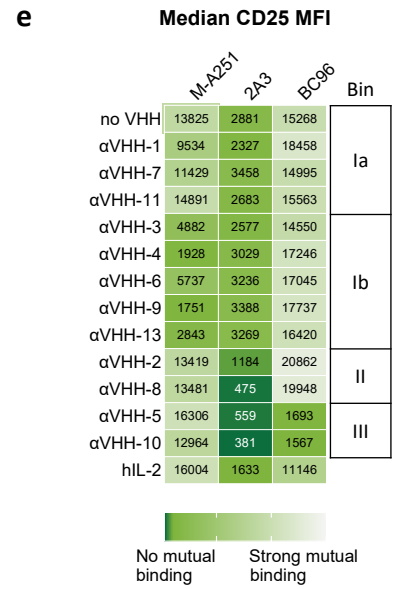

Extended Data Fig. 2d-e | Epitope binning of anti-CD25 VHH antibodies. d, SPR competition binding profiles for anti-CD25 VHHs. VHHs were injected sequentially over a CD25-coated chip: in each cycle first antibody was injected (*), then the second antibody was injected (**). RU values were extracted at 320 s (first injection) and 440 s (second injection) to assess competitive binding. **e**, Flow cytometry–based epitope competition assay using fluorescently labeled commercial anti-CD25 antibodies. HEK$^{\alpha\beta\gamma}$ cells were pre-incubated with 50 nM of individual one-armed VHH-hFc constructs, followed by addition of commercial fluorescently labeled anti-CD25 antibodies at 1:50 dilution. Commercial clones clustered into three epitope groups: M-A251/4E3/7G7B6, 2A3/MEM-181/3G10/ITYV and BC96 (results for representative clones are shown).

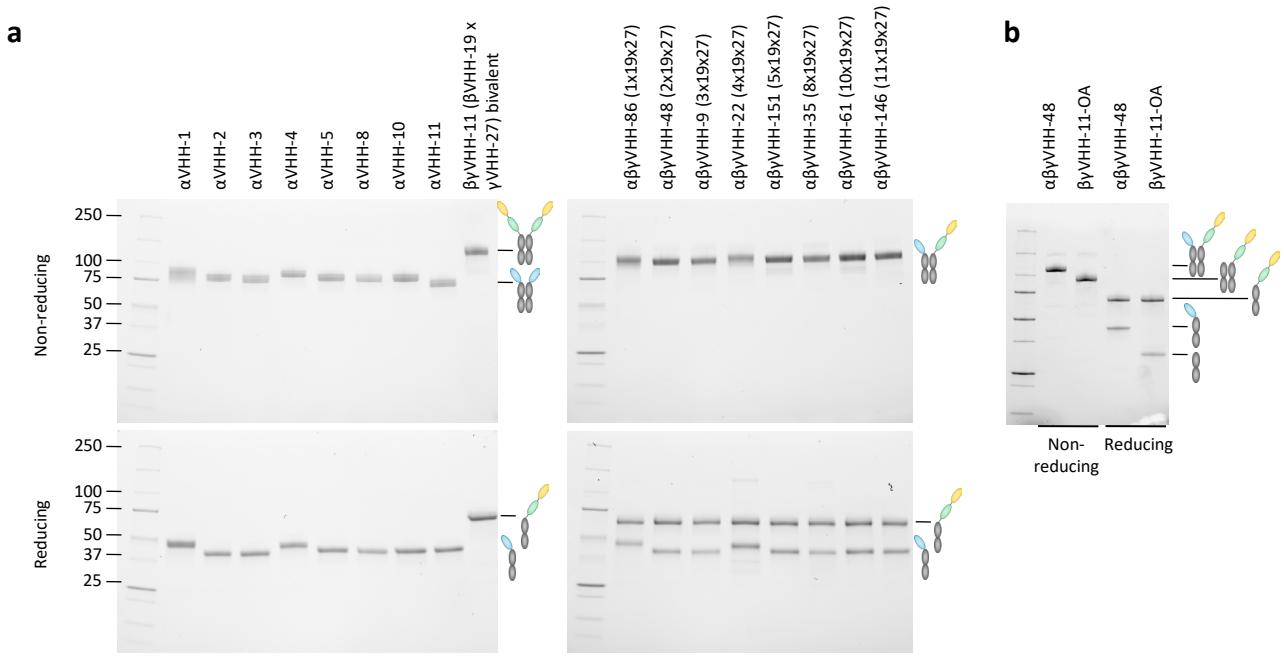

Extended Data Fig. 3 | Characterization of the selected trispecific anti-IL-2Rαβγ antibodies. a, SDS-PAGE of the monospecific αVHH (~80 kDa full antibody and ~40 kDa for two identical heavy chains), bispecific βγVHH-11 (110 kDa full antibody and 55 kDa for two identical heavy chains), and the derived trispecific αβγVHHs (93 kDa full antibody and 55 and 36 kDa for two heavy chains), which were used for cell-based assays. **b**, SDS-PAGE of the trispecific αβγVHH-48 and its parental bispecific βγVHH-11-OA, which were used for in vivo studies. MW marker (kD) was loaded in the left lane of each gel.

a

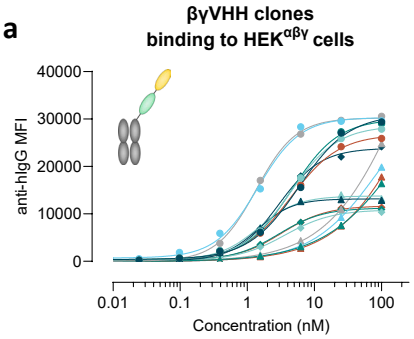

VHH clone	EC50 (nM)
BsVHH-1 (16x27)	5.9
BsVHH-2 (16x31)	4.3
BsVHH-3 (16x32)	4.7
BsVHH-5 (16x36)	4.5
BsVHH-21 (26x27)	1.4
BsVHH-22 (26x31)	1.4
BsVHH-23 (26x32)	1.4
BsVHH-25 (26x36)	1.5
BsVHH-11 (19x27)	371
BsVHH-12 (19x31)	94
BsVHH-13 (19x32)	236
BsVHH-15 (19x36)	250
BsVHH-6 (18x27)	2.9
BsVHH-7 (18x31)	3.6
BsVHH-8 (18x32)	2.9
BsVHH-10 (18x36)	3.3

b

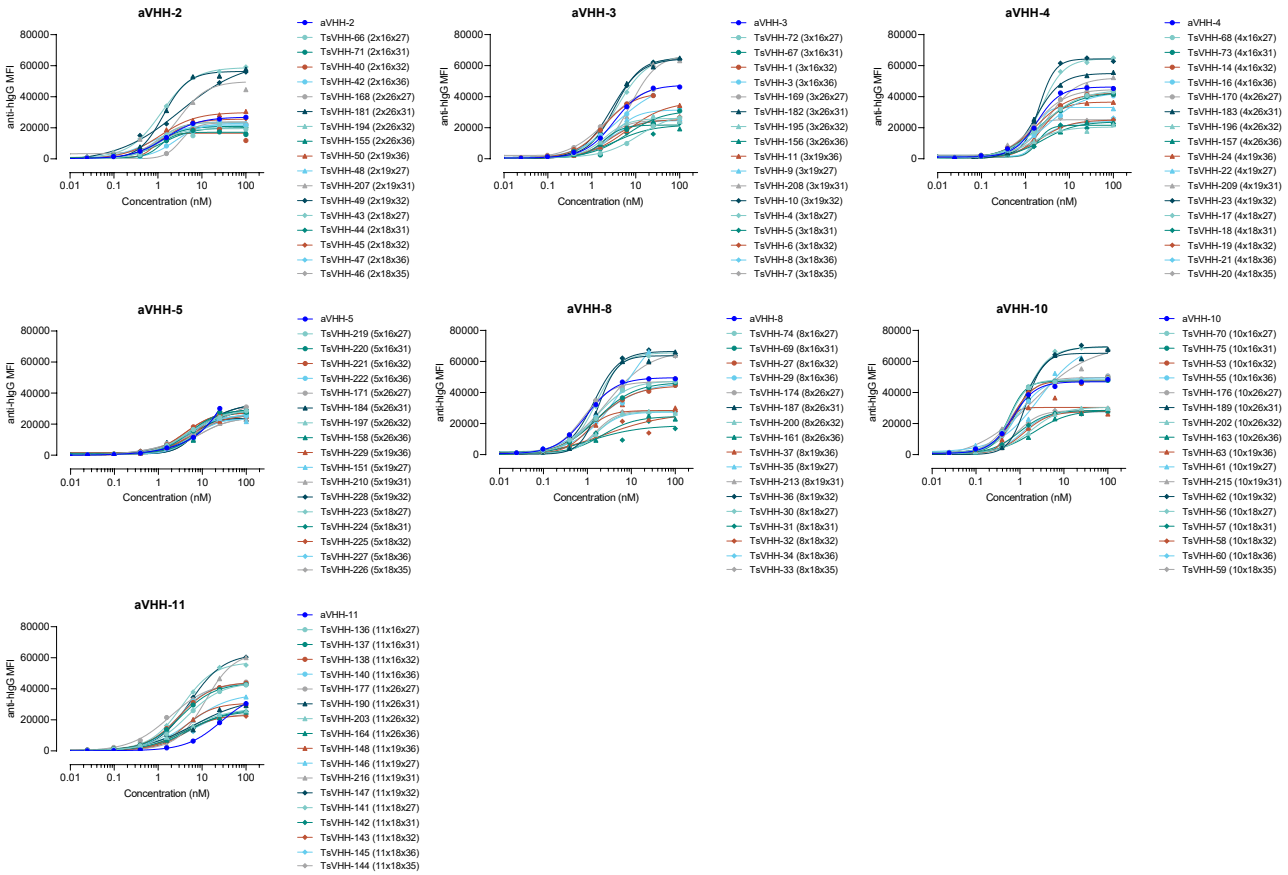

Extended Data Fig. 4 | **Anti-IL-2R antibodies bind to their targets on cells. a**, Dose-response binding curves of selected bispecific monovalent anti-IL-2Rβγ VHH antibodies to HEK^{αβγ} cells as measured by flow cytometry. Detection with PE-labelled anti-human IgG. One independent experiment of two is shown. **b**, Dose-response binding curves of selected trispecific anti-IL-2Rαβγ VHH antibodies to HEK^{αβγ} as measured by flow cytometry. Detection with PE-labelled anti-human IgG. One independent experiment of two is shown.

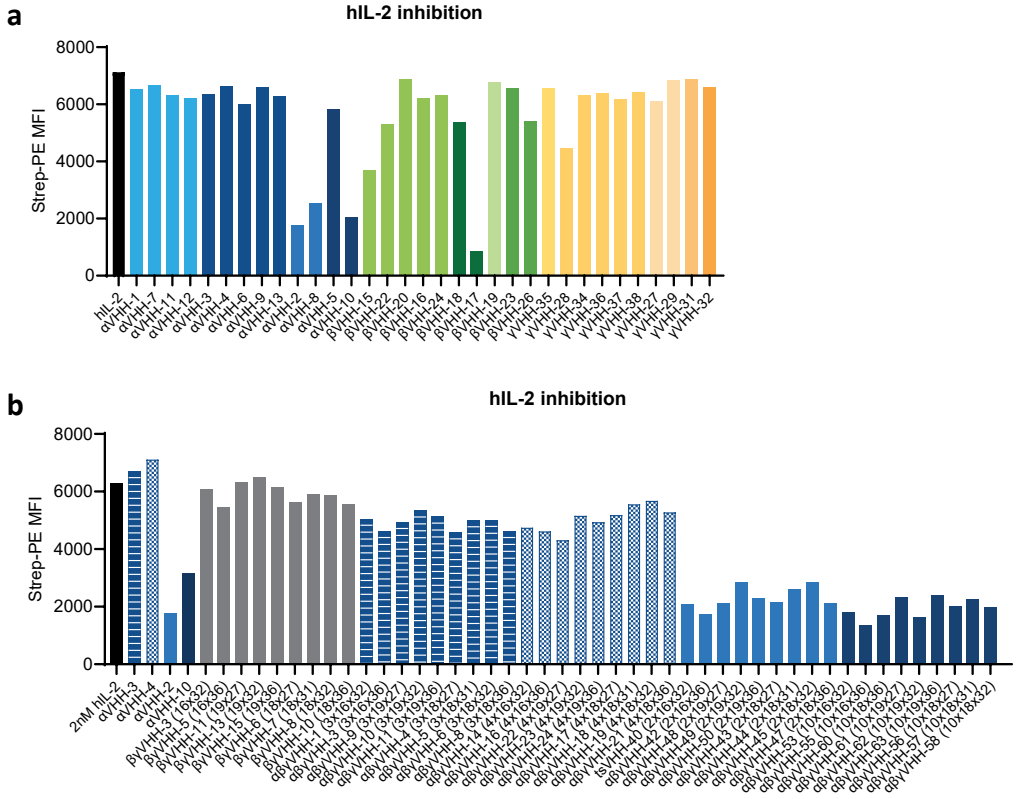

Extended Data Fig. 5 | **Some anti-IL-2R mAbs block the binding of hIL-2 to its receptor. a**, Ability of selected monospecific VHH antibodies binding IL-2R α-, β-, or γ-chain to neutralise the binding of biotinylated IL-2 to HEK$^{\alpha\beta\gamma}$ cells as measured by flow cytometry. Antibodies were added to cells at 10 nM for 15 minutes, followed by addition of 2nM biotinylated human IL-2 for 1 hour. Detection with PE-labelled streptavidin. Color coding per epitope bin for each receptor subunit: IL-2Rα binders in shades of blue, IL-2Rβ binders in shades of green, IL-2Rγ binders in shades of yellow. **b**, Ability of monospecific, bispecific and trispecific anti-IL-2R antibodies to inhibit binding of IL-2 to HEK$^{\alpha\beta\gamma}$ cells as measured by flow cytometry. No test antibody was added in the condition "2nM hIL-2". Bispecific IL-2Rβγ binders in grey; trispecific clones containing the same anti-IL-2Rα VHH are similarly colored.

a

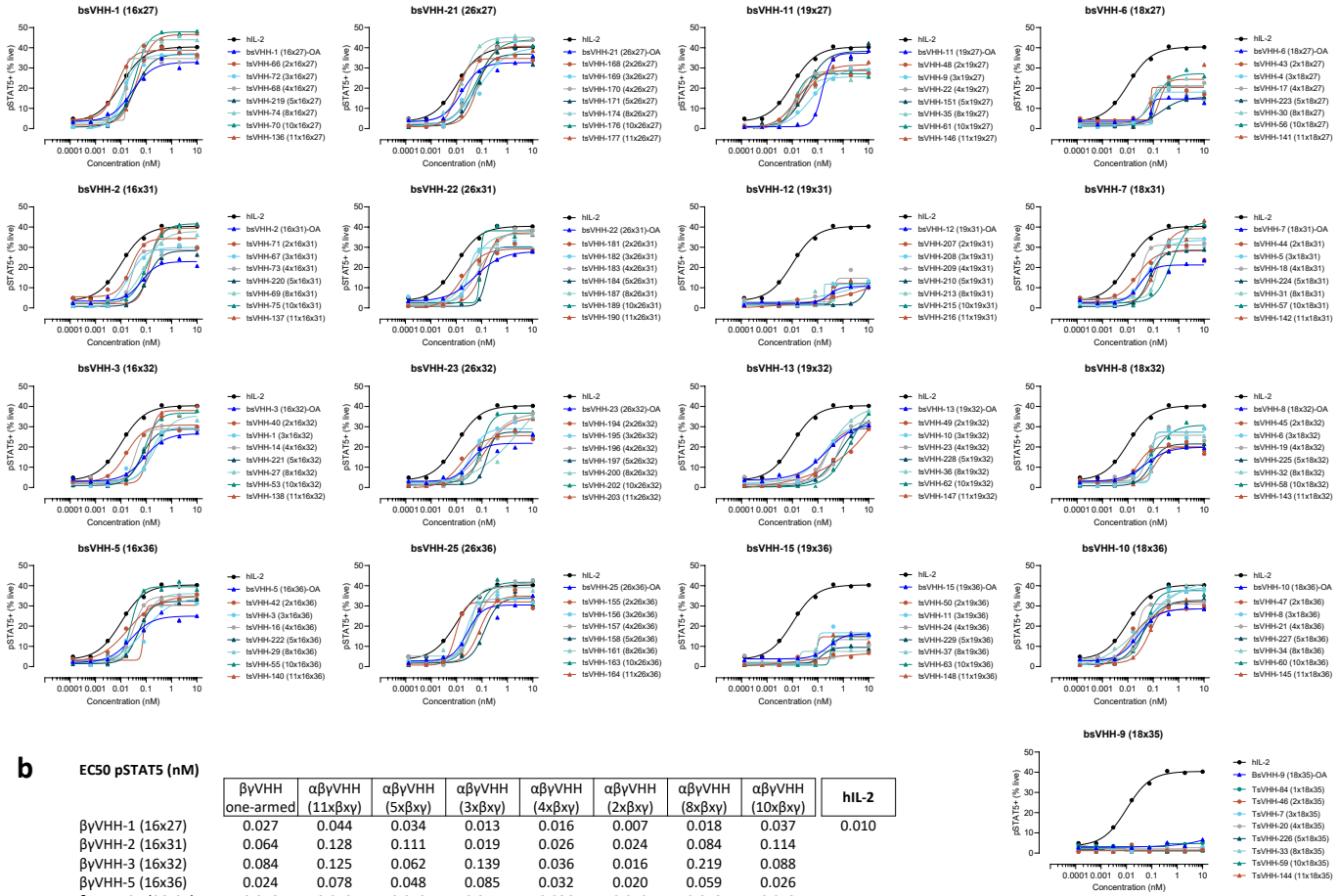

b

EC50 pSTAT5 (nM)

	βγVHH one-armed	αβγVHH (11xβxγ)	αβγVHH (5xβxγ)	αβγVHH (3xβxγ)	αβγVHH (4xβxγ)	αβγVHH (2xβxγ)	αβγVHH (8xβxγ)	αβγVHH (10xβxγ)	hIL-2
βγVHH-1 (16x27)	0.027	0.044	0.034	0.013	0.016	0.007	0.018	0.037	0.010
βγVHH-2 (16x31)	0.064	0.128	0.111	0.019	0.026	0.024	0.084	0.114	
βγVHH-3 (16x32)	0.084	0.125	0.062	0.139	0.036	0.016	0.219	0.088	
βγVHH-5 (16x36)	0.024	0.078	0.048	0.085	0.032	0.020	0.059	0.026	
βγVHH-21 (26x27)	0.016	0.070	0.050	0.075	0.036	0.010	0.018	0.059	
βγVHH-22 (26x31)	0.057	0.109	0.153	0.029	0.087	0.017	0.034	0.087	
βγVHH-23 (26x32)	0.031	0.131	0.150	0.036	0.107	0.017	na	0.093	
βγVHH-25 (26x36)	0.026	0.081	0.126	0.024	0.057	0.009	0.038	0.050	
βγVHH-11 (19x27)	0.152	0.027	0.035	0.057	0.016	0.015	0.011	0.012	
βγVHH-12 (19x31)	0.286	0.335	na	na	0.447	na	na	0.432	
βγVHH-13 (19x32)	0.218	0.194	0.707	0.210	0.647	na	0.306	1.837	
βγVHH-15 (19x36)	0.263	0.088	0.145	0.091	0.453	0.055	0.019	0.327	
βγVHH-6 (18x27)	0.085	0.168	0.200	0.099	0.061	0.080	0.107	0.111	
βγVHH-7 (18x31)	0.030	0.137	0.069	0.057	0.033	0.024	0.146	0.509	
βγVHH-8 (18x32)	0.049	0.112	0.079	0.088	0.054	0.025	0.092	0.089	
βγVHH-10 (18x36)	0.026	0.071	0.040	0.039	0.024	0.013	0.041	0.049	

c

EC50 fold change tsVHH/bsVHH

	αβγVHH (11xβxγ)	αβγVHH (5xβxγ)	αβγVHH (3xβxγ)	αβγVHH (4xβxγ)	αβγVHH (2xβxγ)	αβγVHH (8xβxγ)	tsVHH (10xβxγ)
βγVHH-1 (16x27)	1,7	1,3	0,5	0,6	0,3	0,7	1,4
βγVHH-2 (16x31)	2,0	1,7	0,3	0,4	0,4	1,3	1,8
βγVHH-3 (16x32)	1,5	0,7	1,6	0,4	0,2	2,6	1,0
βγVHH-5 (16x36)	3,2	2,0	3,5	1,3	0,8	2,5	1,1
βγVHH-21 (26x27)	4,4	3,2	4,7	2,3	0,6	1,1	3,7
βγVHH-22 (26x31)	1,9	2,7	0,5	1,5	0,3	0,6	1,5
βγVHH-23 (26x32)	4,1	4,8	1,1	3,4	0,5	na	3,0
βγVHH-25 (26x36)	3,1	4,9	0,9	2,2	0,4	1,5	1,9
βγVHH-11 (19x27)	0,2	0,2	0,4	0,1	0,1	0,1	0,1
βγVHH-12 (19x31)	1,2	na	na	1,6	na	na	1,5
βγVHH-13 (19x32)	0,9	3,2	1,0	3,0	na	1,4	8,4
βγVHH-15 (19x36)	0,3	0,6	0,3	1,7	0,2	0,1	1,2
βγVHH-6 (18x27)	2,0	2,3	1,2	0,7	0,9	1,3	1,3
βγVHH-7 (18x31)	4,6	2,3	1,9	1,1	0,8	4,9	17,2
βγVHH-8 (18x32)	2,3	1,6	1,8	1,1	0,5	1,9	1,8
βγVHH-10 (18x36)	2,7	1,5	1,5	0,9	0,5	1,6	1,9

Extended Data Fig. 6 | pSTAT5 activation by anti-IL-2R antibodies in HEK$^{\alpha\beta\gamma}$ cells. a, pSTAT5 dose-response curves of selected bispecific anti-IL-2Rβγ and trispecific anti-IL-2Rαβγ VHH antibodies in HEK$^{\alpha\beta\gamma}$ cells as measured by flow cytometry analysis. **b**, EC_{50} values for the pSTAT5 activation by selected bispecific anti-IL-2Rβγ and trispecific anti-IL-2Rαβγ clones pictured in (**a**). The EC50 values were determined with dose-response curves generated from the experimental data by a four-parameter logistic fit function (4PL). **c**, Fold-change in EC_{50} (ΔEC_{50}) values between trispecific anti-IL-2Rαβγ clones and their corresponding parental one-armed bispecific anti-IL-2Rβγ.

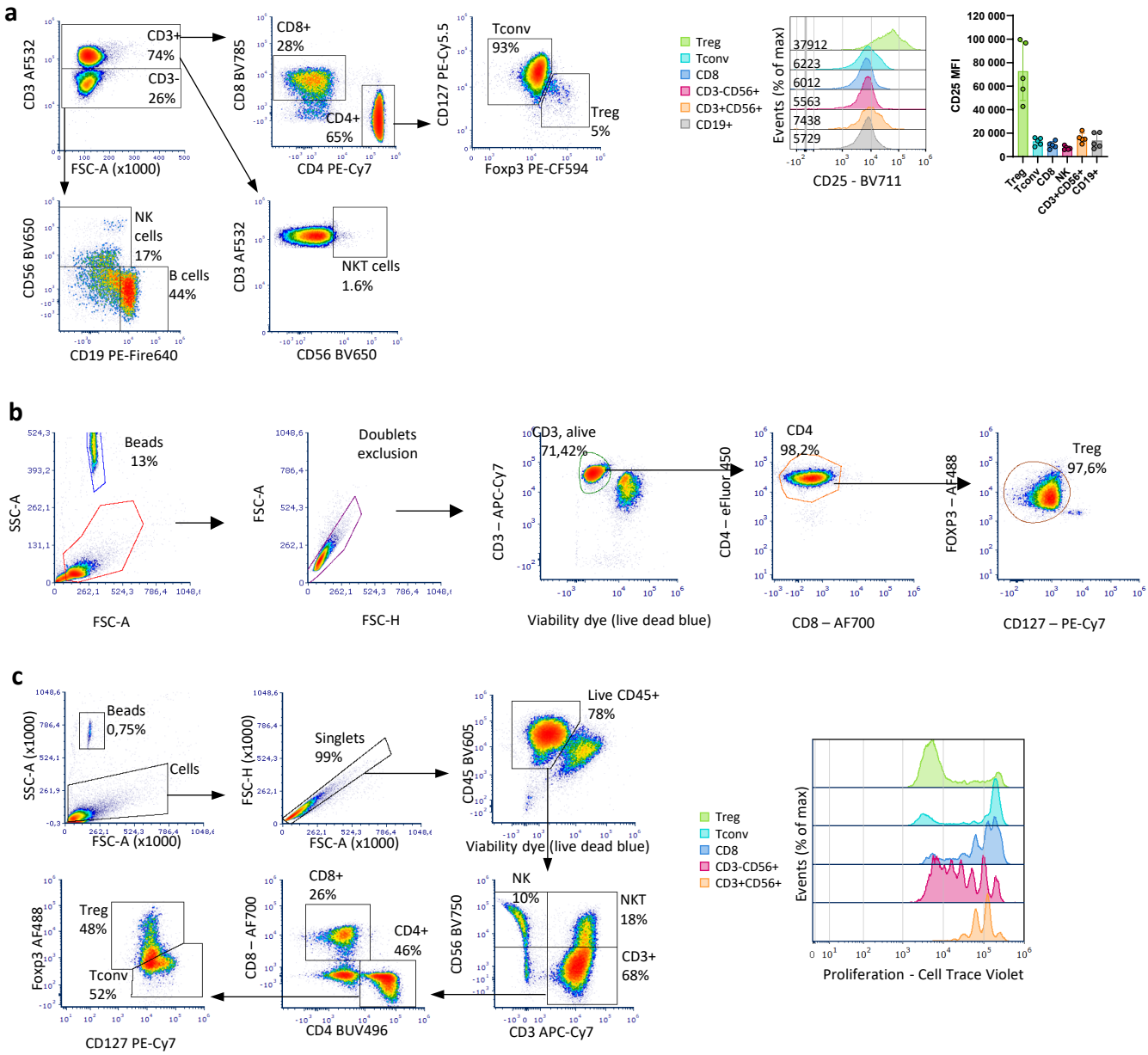

Extended Data Fig. 7 | **pSTAT5 activation by anti-IL-2R antibodies in human PBMC. a**, Gating strategy for ex vivo pSTAT5 assay using human PBMCs, shown in **Fig. 3c**. Sample treated with 100 nM hIL-2; pre-gated on single live cells. CD25 histograms include MFI values for each cell population. **b**, Gating strategy for Treg expansion assay, shown in **Fig.3e**. **c**, Gating strategy and proliferation peaks for ex vivo total PBMC expansion assay, shown in **Fig. 3f**.

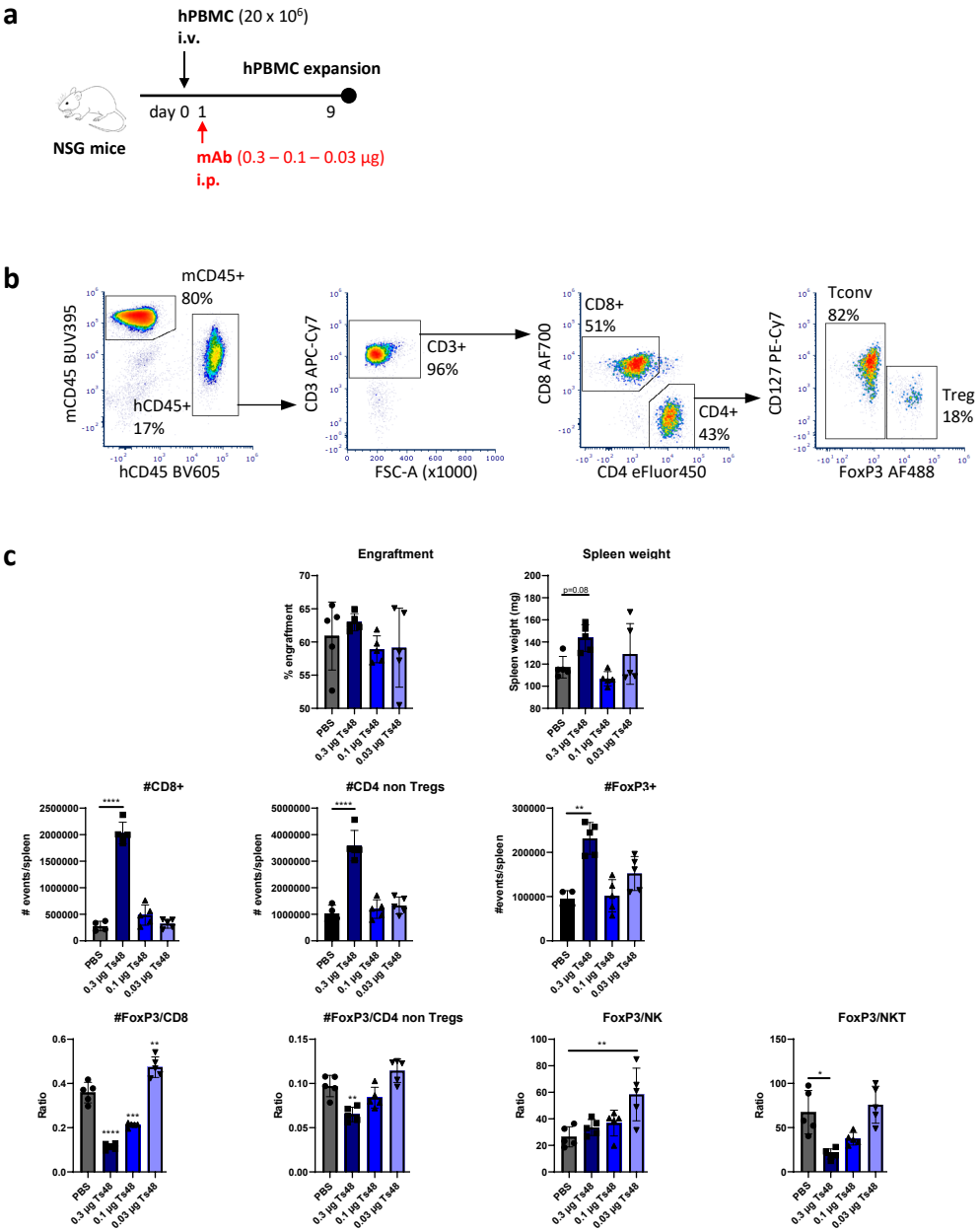

Extended Data Fig. 8 | Setup and optimization of the in vivo NSG expansion model. a, Experimental setup. **b**, NSG expansion model is characterized by rapid expansion of non-Treg populations, while Treg disappear rapidly after day 14. **c**, Gating strategy for the flow cytometric analysis of blood human T cell populations in NSG expansion model. Pre-gated on single live cells. **d**, Optimization experiment to determine the optimal dose of the αβγVHH-48 (denoted "Ts48"). Data are presented as the mean ± s.e.m. with three, four or five mice per group. The *P* values shown were determined by one-way ANOVA (Tukey-Kramer's test). **P* ≤ 0.05, ***P* ≤ 0.01, ****P* ≤ 0.001, *****P* ≤ 0.0001.

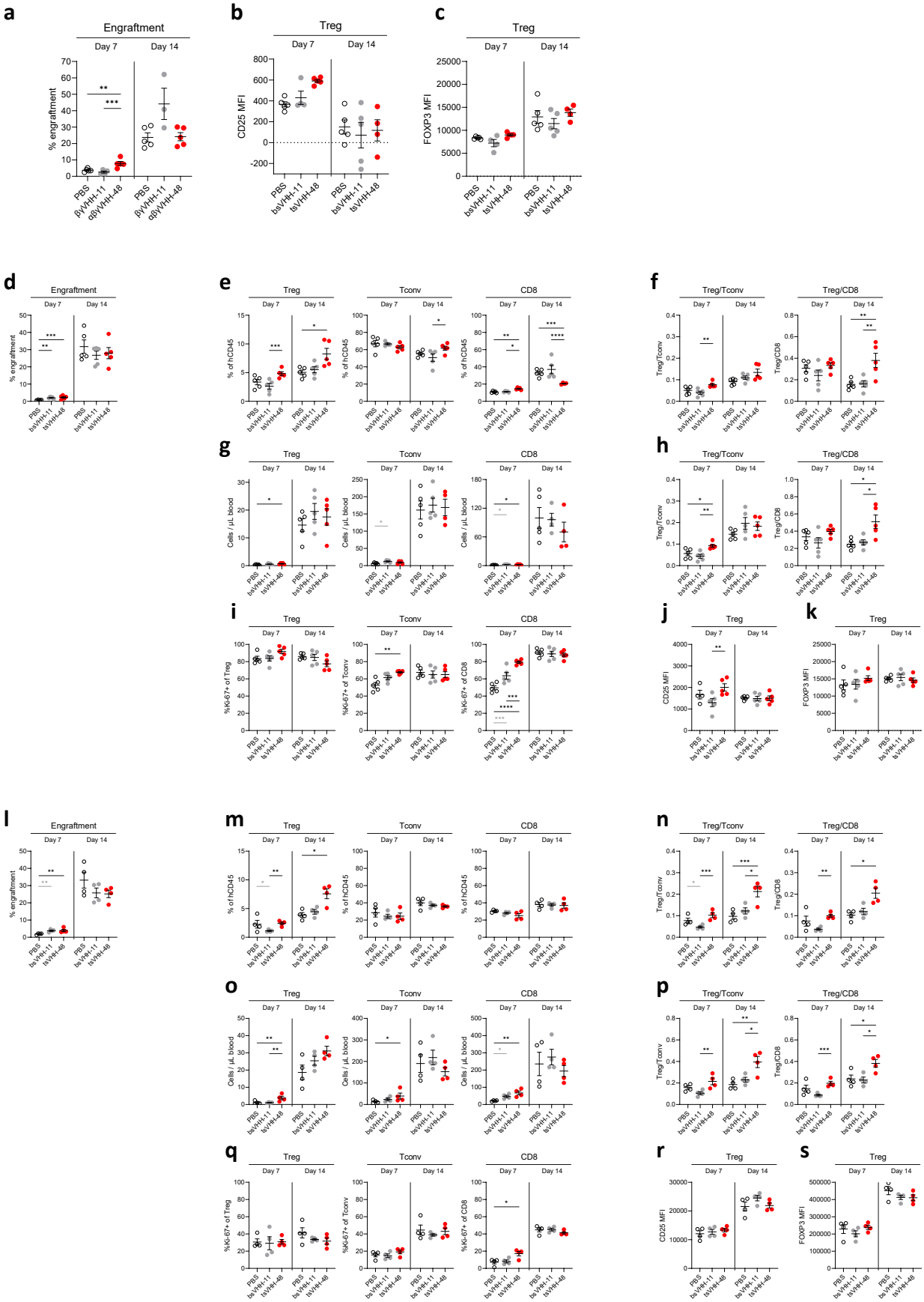

Extended Data Fig. 9 | See next page for caption.

Extended Data Fig. 9 | **TsVHH-48 preferentially increases Treg in an in vivo NSG expansion model.**

a-c, Extra data for the experiment shown in Fig. 4. **a**, Engraftment of human CD45 cells in the animal's blood circulation. **b**, CD25 expression on Treg. **c**, FOXP3 expression on Treg.

d-k, First repeat of the experiment shown in Fig. 4. **d**, Engraftment of human CD45 cells on day 7 and day 14 after the start of the experiment after treatment with either trispecific αβγVHH-48 antibody ("tsVHH-48") or the parental bispecific βγVHH-11 ("bsVHH-11"). **e**, Treg, Tconv and CD8 T cell percentages. **f**, Treg/Tconv and Treg/CD8 T cell number ratios. **g**, Treg, Tconv and CD8 T cell numbers. **h**, Treg/Tconv and Treg/CD8 T cell number ratios. **i**, Percentages of Ki-67$^+$ cells among Treg, Tconv and CD8 T cells. **j**, CD25 expression on Treg cells. **k**, FOXP3 expression on Treg cells.

l-s, Second repeat of the experiment shown in Fig. 4. **l**, Engraftment of human CD45 cells on day 7 and day 14 after the start of the experiment after treatment with either trispecific αβγVHH-48 antibody ("tsVHH-48") or the parental bispecific βγVHH-11 ("bsVHH-11"). **m**, Treg, Tconv and CD8 T cell percentages. **n**, Treg/Tconv and Treg/CD8 T cell number ratios. **o**, Treg, Tconv and CD8 T cell numbers. **p**, Treg/Tconv and Treg/CD8 T cell number ratios. **q**, Percentages of Ki-67$^+$ cells among Treg, Tconv and CD8 T cells. **r**, CD25 expression on Treg cells. **s**, FOXP3 expression on Treg cells.

Data are presented as the mean ± s.e.m. with three, four or five mice per group. The *P* values shown were determined by one-way ANOVA (Tukey-Kramer's test). **P* ≤ 0.05, ***P* ≤ 0.01, ****P* ≤ 0.001, *****P* ≤ 0.0001.

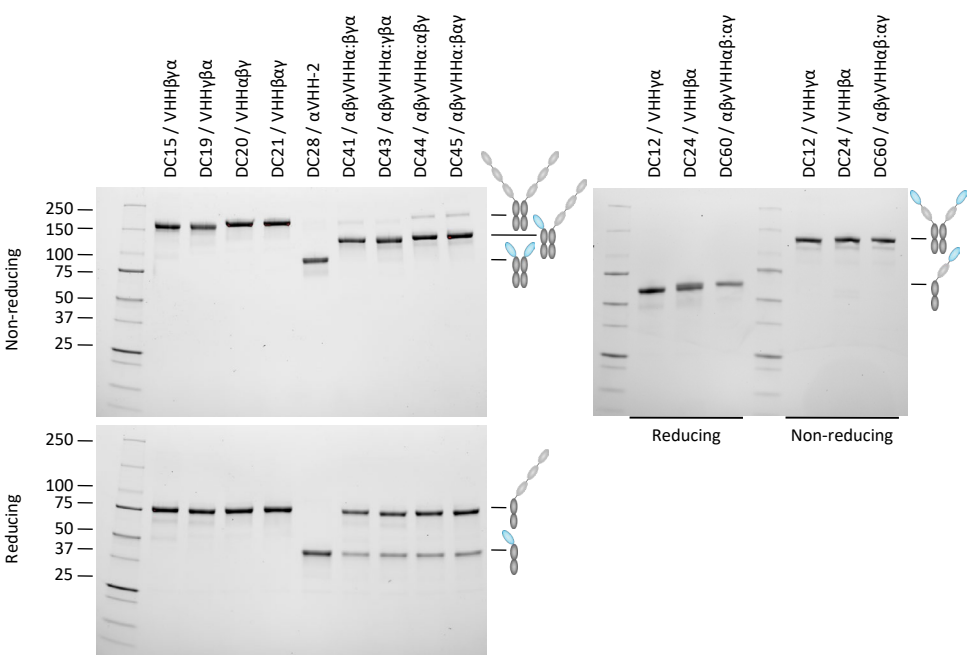

Extended Data Fig. 10 | **Characterization of the trispecific anti-IL-2Rαβγ antibodies. a**, SDS-PAGE of the trispecific αβγVHH with optimized geometries. MW marker (kD) was loaded in the left lane of each gel.